J. Fluid Mech. (2004), *vol.* 518, *pp.* 231–259. © 2004 Cambridge University Press
DOI: 10.1017/S0022112004001004 Printed in the United Kingdom

Extinction and reignition in a diffusion flame: a direct numerical simulation study

By PAIBOON SRIPAKAGORN[1], SATOSHI MITARAI[1], GEORGE KOSÁLY[1] AND HEINZ PITSCH[2]

[1]Department of Mechanical Engineering, University of Washington, Seattle, WA 98195-2600, USA
[2]Center for Turbulence Research, Stanford University, Stanford, CA 94305-3030, USA

(Received 22 October 2002 and in revised form 8 July 2004)

The goal of this study is to provide a window into the physics of extinction and reignition via three-dimensional simulations of non-premixed combustion in isotropic decaying turbulence using one-step global reaction and neglecting density variations. Initially non-premixed fields of fuel and oxidant are developing in a turbulent field. Due to straining, the scalar dissipation rate is initially increasing and its fluctuations create extinguished regions on the stoichiometric surface. Later in the process, the stoichiometric surface again becomes uniformly hot. Besides using Eulerian data, this research applies flame element tracking and investigates the time history of individual points ('flame elements') along the stoichiometric surface. The main focus of the study is the discussion of the different scenarios of reignition. This paper identifies three major scenarios: independent flamelet scenario, reignition via edge (triple) flame propagation, and reignition through engulfment by a hot neighbourhood. The results give insight into the role different scenarios play in the reignition process, reveal the physical processes associated with each scenario, and provide the relative frequency of reignition for each scenario.

1. Introduction

The central problem in the modelling of turbulent diffusion flames is the coupling of turbulence with chemistry. The two main approaches presently available are (a) mixture-fraction-based modelling (conditional moment closure, flamelet), and (b) Monte-Carlo probability density function (PDF) modelling. A discussion of these models can be found in two recent books by Peters (2000) and by Poinsot & Veynante (2001). It can be concluded from these discussions that the mean composition fields of simple, parabolic jets with continuous combustion (i.e. without a significant amount of extinction) are basically well-predicted by both approaches. Practical flames, however, often exhibit extinction and reignition behaviour. This phenomenon appears in the laboratory, e.g. in connection with piloted jet flames at high strain rate values (Barlow & Frank 1998). The strain may cause local extinction near the flame base, but the presence of the pilot prevents liftoff and blowout. As strain relaxes further away from the nozzle, reignition occurs.

Present day mixture-fraction-based models cannot predict local extinction and reignition behaviour. Monte-Carlo PDF is capable of modelling extinction and reignition (Xu & Pope 2000; Lindstedt, Louloudi & Váos 2000) but the quality of the prediction depends sensitively on the mixing model applied and the values of the constants used in these models. This is an ad hoc element of the approach. Regarding

https://doi.org/10.1017/S0022112004001004 Published online by Cambridge University Press

mixture-fraction-based modelling, the major difficulty is related to reignition, which cannot be described without accounting for the interaction between local cold spots and the hot environment. This issue has been recently investigated by Hewson & Kerstein (2002).

The direct numerical simulation (DNS) data presented in this paper are intended to provide a window into the physics of extinction and reignition. The paper reports on the three-dimensional DNS of initially non-premixed fields of fuel and oxidant developing in an isotropic decaying turbulent field using one-step global reaction and neglecting density variations. Due to straining, the scalar dissipation rate is initially increasing and this leads to local extinction events. Local extinction and reignition are governed by the interplay of mixing and reaction. Overholt & Pope (1999) conclude in a recent DNS study that, in the absence of local extinction, the conditional moment closure based on the local scalar dissipation rate gives good agreement with the data. This conclusion is the starting point of the present study. The DNS data do indeed show that, in the absence of extinction and reignition, the steady flamelet model represents correctly the simulated data. Based on this observation this paper defines extinction and reignition vis-á-vis steady flamelet behaviour. Extinction and reignition are considered as deviations from the burning solutions of the steady flamelet equation, followed by a gradual return to it.

The study focuses on the deviations from the steady flamelet solution. Besides looking at the fields in the laboratory system (Eulerian data), the paper applies the technique of 'flame element tracking' that shows the fields as they would appear in a local coordinate system fixed to a point on the instantaneous stoichiometric surface. This approach was introduced by Mell *et al.* (1994) and is a key element of the present work. The data obtained from tracking, together with highly resolved DNS, make possible the study of the detailed physics of extinction and reignition phenomena.

The numerical experiment is described in § 2. Section 3 discusses flame element tracking and reviews the fundamental ideas of flamelet modelling. The main results of the paper are presented and discussed in § 4. The conclusions of the study, together with some discussion of future directions, appear in § 5.

2. Numerical experiment

2.1. *Physical problem description*

The phenomena under investigation are the extinction and reignition of non-premixed combustion under the changing balance between mixing and reaction. The numerical experiment was performed via DNS involving five scalars: three velocity components, one conserved scalar and one reacting scalar. The simulated velocity field is incompressible decaying isotropic turbulence comparable to the turbulence downstream of a laboratory grid. The initialization of the scalars is based on 'blobs' that are homogeneously distributed in space. The two scalars computed in the simulations are the mixture fraction, Z, and the reacting scalar, Θ (to be defined later).

For the present case, on the average, reaction is faster than mixing. This leads to cases where, globally, the mass fractions are close to equilibrium at all times. However, due to strong fluctuations of turbulent mixing and the high activation energy of the global reaction, local extinction occurs. Local extinction and reignition are governed by the interplay of mixing and reaction.

The local mixing time is characterized by the inverse of the scalar dissipation rate, χ, defined as $2D|\nabla Z|^2$ where D is the coefficient of molecular diffusion. In figure 1, χ_q indicates the highest value of the scalar dissipation rate at the stoichiometric value

https://doi.org/10.1017/S0022112004001004 Published online by Cambridge University Press

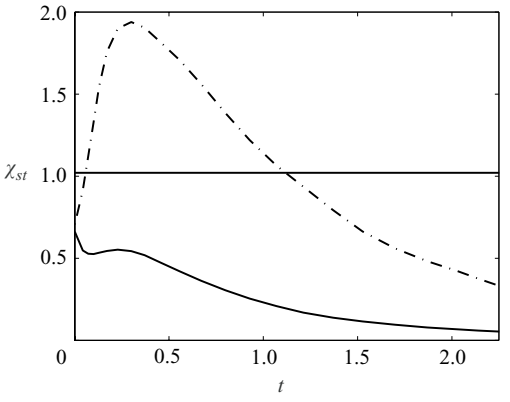


FIGURE 1. The time evolution of the scalar dissipation rate at $Z = Z_{st} = 0.5$ (χ_{st}). Full line: $\langle \chi_{st} \rangle$, dash-dot line: the envelope that contains 99% of the fluctuations of χ_{st}. The horizontal line is drawn at $\chi_{st} = \chi_q = 1.04$. This is the largest possible value of χ_{st} for which the steady flamelet equation has a burning solution. The numerical value refers to the chemistry parameters shown in table 2.

of the mixture fraction, χ_{st}, where the steady flamelet model (3.3) has a burning solution. The inverse of the extinction threshold, χ_q, is thus a relevant chemistry time scale (Bray & Peters 1994). Note that the time (t) used in the presentation of the data is the simulation time normalized by the initial large-eddy turnover time (l_0/u_0') where l_0 and u_0' are the initial integral length scale and r.m.s. velocity.

The reacting field is initialized with solutions of the steady flamelet equation. Initially, $\chi_{st} < \chi_q$ along the entire stoichiometric surface, so that the whole surface is burning. Once the scalars have been injected, turbulent strain creates large scalar gradients. Due to the many different turbulent scales involved in the straining, the scalar dissipation rate fluctuates strongly. To focus attention on the reaction zone, figure 1 shows the time evolution of the scalar dissipation rate, χ, at $Z = Z_{st}$. The average of χ_{st} stays lower than χ_q throughout the simulation. However, early in the simulations, some of the fluctuating values of χ_{st} far exceed the critical threshold leading to local extinction. Figure 1 shows that local extinction is due to the fluctuations of the scalar dissipation rate. After a while, molecular mixing overcomes the influence of turbulent straining and leads to the decrease of the scalar gradients. This process is accompanied by gradual reignition; ultimately the reacting scalar field returns to the steady flamelet solution. This paper examines local extinction and reignition phenomena caused by the increase and subsequent decrease of the scalar dissipation rate illustrated in figure 1.

2.2. *Direct numerical simulation (DNS)*

The main parameters of the initial velocity and scalar fields are shown in table 1. The goal is to simulate a fully developed homogeneous and isotropic field with the largest Reynolds number achievable in the computational volume considered. To achieve this goal under numerical constraints, the initial velocity field developed by Nilsen & Kosály (1999) has been used. The velocity field is created from a prescribed energy spectrum and allowed to evolve according to the Navier–Stokes equations until conditions characterizing fully developed turbulent flow, undergoing full spectrum decay, are met. At the time when the scalars are initialized, all the characteristic length scales of the velocity field increase with time and the velocity

https://doi.org/10.1017/S0022112004001004 Published online by Cambridge University Press

$k_{\max}\eta_k$	l/η_k	u'/l	Re_l	Re_λ	N	Sc
3.88	27	1.015	78	32	256^3	0.7

TABLE 1. Initial conditions used in the DNS of the flow field and the mixture fraction field. $k_{\max}\eta_k$ is the product of the cutoff wavenumber and the Kolmogorov scale indicative of the spatial resolution, l/η_k the initial length scale ratio, u'/l the initial large eddy strain rate, Re_l the initial Reynolds number based on the initial velocity scales, Re_λ the initial Taylor Reynolds number, N the number of grid points, and Sc the Schmidt number.

derivative skewness is at its maximum value. In this study, the initial Reynolds number based on the Taylor scale, Re_λ, is 32. Initially l/η_k is 27, where η_k is the Kolmogorov length scale. At the end of the simulation, $l/\eta_k = 16$. A single-step reversible reaction has been considered with an Arrhenius-type rate coefficient:

$$\mathrm{F} + r\mathrm{O} \leftrightharpoons (r+1)\mathrm{P} \tag{2.1}$$

For a two-feed problem with simple chemistry, the mixture fraction is defined by

$$Z = \frac{rY_F - Y_O + Y_{O\infty}}{rY_{F\infty} + Y_{O\infty}}. \tag{2.2}$$

Here r is the stoichiometric ratio, i.e. the mass of oxidant disappearing with unit mass of fuel; Y_F, Y_O and Y_P stand for the mass fractions of fuel, oxidant, and product, respectively. The unmixed values of the fuel and oxidant mass fractions ($Y_{F\infty}$, $Y_{O\infty}$) are unity, therefore the stoichiometric value of the mixture fraction is $Z_{st} = 1/(r+1)$. The present choice is $r = 1$, which means $Z_{st} = 0.5$. Using an equilibrium constant, K, to represent reversible chemistry, the production rate of the product can be written (Lee & Pope 1995)

$$w_P = (r+1)A \exp\left(\frac{-\beta}{\alpha}\right) \exp\left[\frac{-\beta(1-Y_P)}{1-\alpha(1-Y_P)}\right] \left(Y_F Y_O - \frac{1}{K} Y_P^{r+1}\right). \tag{2.3}$$

The global reaction is characterized by the pre-exponential factor A and the following dimensionless quantities:

$$\text{heat-release parameter,} \quad \alpha = \frac{T_b - T_u}{T_b}, \tag{2.4a}$$

$$\text{Zeldovich number,} \quad \beta = \frac{T_a}{T_b}\frac{T_b - T_u}{T_b}, \tag{2.4b}$$

where T_a is the activation temperature, T_b is the adiabatic flame temperature, and T_u is the temperature of both the unburned fuel and the oxidant. The normalized temperature, Θ, is defined as

$$\Theta = \frac{T - T_u}{T_b - T_u}. \tag{2.5}$$

Table 2 shows the values of the thermochemistry parameters used in this study. The parameters were selected to make the reaction rate strongly temperature dependent and lead to local extinction in a strongly burning flame (de Bruyan Kops 1999). The parameters result in the extinction threshold $\chi_q = 1.04$. The choice of the Zeldovich number will be discussed in § 2.3.

The initial mixture fraction is arranged in blobs of fuel and oxidant ($Z = 1$ and $Z = 0$). The fuel blobs fill approximately half of the computational domain and thus

https://doi.org/10.1017/S0022112004001004 Published online by Cambridge University Press

r	A	α	β	K
1.0	80000	0.87	4.0	100

TABLE 2. Numerical values of the thermochemistry parameters defined in § 2.2.

the average value of the mixture fraction, $\langle Z \rangle$, is close to 0.5. For single-step chemistry each mass fraction together with the mixture fraction determine the other two mass fractions. The product mass fraction, Y_P, is equal to the normalized temperature Θ. The scalar Θ and Z were chosen to characterize the reacting field. The Schmidt number ($Sc = \nu/D$) is 0.7 for both Z and Θ. Here ν is the kinematic viscosity.

In the steady flamelet model (Peters 1984) the mass fractions depend on space and time through the local instantaneous value of mixture fraction Z and scalar dissipation rate χ. The temperature field Θ is initialized via the steady flamelet model.

The simulated velocity field evolves according to the incompressible Navier–Stokes equations,

$$\nabla \cdot \boldsymbol{u} = 0, \tag{2.6a}$$

$$\frac{\partial \boldsymbol{u}}{\partial t} = \boldsymbol{u} \times \boldsymbol{\omega} - \nabla\{p - \tfrac{1}{2}|\boldsymbol{u}^2|\} + \nu \nabla^2 \boldsymbol{u}, \tag{2.6b}$$

where $\boldsymbol{\omega}$ denotes the vorticity vector and p is the static hydrodynamic pressure. The kinematic viscosity is taken to be independent of the temperature.

The mixture fraction and species mass fractions satisfy the conservation equation

$$\frac{\partial Y_i}{\partial t} = -\boldsymbol{u} \cdot \nabla Y_i + D \nabla^2 Y_i - w_i. \tag{2.7}$$

In the Z-equation the reaction rate is zero.

The set of governing equations was solved using a pseudo-spectral code developed by Nilsen (1998). The computational domain is a cube with periodic boundaries to facilitate Fourier transformation. The spatial derivative fields were evaluated in Fourier space while nonlinear terms such as $\boldsymbol{u} \times \boldsymbol{\omega}$ or $\boldsymbol{u} \cdot \nabla Y_i$ were computed in physical space. Time was advanced by a second-order Adams–Bashforth scheme.

We discuss now two major simplifications in our DNS. Clearly neither the assumption of constant-density flow nor the consideration of only one chemical step are fully appropriate to investigate extinction and reignition of practical flames. Unfortunately, accounting for temperature dilatation is inconsistent with the periodic boundary conditions our code is using. Even more importantly, flame element tracking requires unusually high resolution and this requirement is inconsistent with accounting for true combustion chemistry. A possible choice that would have allowed accounting for both effects would have been to consider two-dimensional cases, instead of working with three spatial dimensions. In fact many authors follow this avenue, precisely because they want to use realistic chemistry schemes and account for density dilatation. (See, e.g., numerous references in the recent textbook of Poinsot & Veynante 2001.) Note that our group has an earlier publication that accounts for density dilatation and radicals in a three-dimensional DNS (Montgomery, Kosály & Riley 1993). The resolution that can be achieved is not sufficient for flame element tracking.

https://doi.org/10.1017/S0022112004001004 Published online by Cambridge University Press

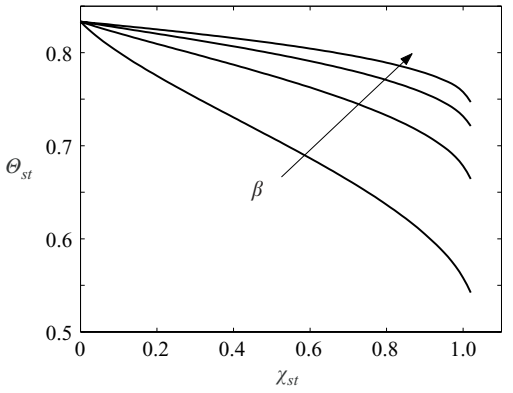


FIGURE 2. Burning solutions of the steady flamelet equation for different values of Zeldovich number, β, but the same value of χ_q ($\chi_q = 1.04$). The temperature and the scalar dissipation rate both refer to stoichiometric mixture. The value of β increases from bottom to top ($\beta = 2.0$, 4.0, 6.0 and 8.0).

The focus of this paper is the investigation of the influence of turbulent mixing on reignition. We consider reignition to be primarily due to thermal interaction between the cold spots and the hot environment. It is the heat flowing toward the extinguished spots that drives the chemistry. How to model this, what are the details and the conditions of this crucial heat transfer, and how it depends on the turbulence and the strain are the questions we are trying to answer. Due to the essentially three-dimensional nature of the eddy dynamics it is impossible to investigate these issues using only two spatial dimensions, which is why we have been forced to simplify the approach quite radically. Note that the opposite simplification (two-dimensional eddies with thermal dilatation and radicals) is equally justified. We believe that the phenomenon under investigation could be investigated using several complementary approaches, ours being one of them.

2.3. *Resolution considerations*

The resolution of the simulations is influenced by the parameters of the three main ingredients: velocity field, scalar field, and chemistry scheme.

To resolve the velocity and conserved scalar field (with order-one Schmidt number), a well-established requirement is $k_{\max}\eta_k > 1$ (Eswaran & Pope 1988). Here $k_{\max}$ is the cutoff wavenumber given by $(15/32)N$ with N being the number of grid points along one direction of the computational domain. The above requirement refers to global averages, the present work requires much better resolution and uses $k_{\max}\eta_k = 3.88$ initially (see table 1). Due to the increase of the length scales the value of $k_{\max}\eta_k$ increases in time. The resolution of the scalar fields is improved further by the choice of $Sc = 0.7$.

For reacting scalars, the stiffness of the chemistry scheme and the interaction between mixing and reaction are further complicating factors. Recently de Bruyn Kops (1999) has investigated the spatial resolution of a DNS configured similarly to the present study, and found that the resolution depends sensitively on the choice of the activation temperature. The choice of the Zeldovich number (β) is a critical step in the design of a numerical experiment.

In figure 2 the normalized temperature is plotted against the scalar dissipation rate, both quantities referring to a stoichiometric mixture. The plots shown in figure 2

https://doi.org/10.1017/S0022112004001004 Published online by Cambridge University Press

represent the burning solution of the steady flamelet equation for different values of β. For each β value a matching value of the pre-exponential factor (A) was chosen such that $\chi_q = 1.04$ in all four cases. Note that the equilibrium value of the temperature (its value as $\chi_{st} \to 0$) is less than unity due to reversibility. The plots show that, for large values of β, extinction takes place more abruptly. One-step chemistry models of different hydrocarbon/oxygen reactions use quite large values of β (Turns 1996). On the other hand, large β values lead to thin reaction zones that tend to jeopardize resolution.

After much experimentation, it has been concluded that choosing $\beta = 4$ is a reasonable compromise between more realistic values and the resolution requirements, and this value was used throughout this study. To generate a sense of the consequences of this choice the main results ($\beta = 4$) will be compared with those of $\beta = 2$ and $\beta = 6$ computations (see figure 9). Comments on the possible influence of using higher values of β will be made at the end of § 4.

Turbulent reacting flows contain a wide range of length scales and time scales. The spatial resolution is determined by the cutoff wavenumber ($k_{\max}$) which in the present simulation was equal to 120. To investigate possible resolution errors, the results reported in this study were compared to results from another simulation using the same computational domain but with $k_{\max} = 85$. Note that this second (less resolved) simulation uses the same input data as given in tables 1 and 2, except that the initial value of $k_{\max}\eta_k$ changes from 3.88 to 2.75. Detailed comparison of the two computations shows minor differences that are inconsequential regarding the conclusions of the present study. The current simulations are considered adequately resolved for the present purposes. To determine the time stepping needed to resolve the multitude of time scales in the reacting turbulence, the simple method of reducing the time steps by half is used until the results become consistent.

3. Diagnostic tools and flamelet modelling

3.1. *Flame element tracking*

Unless the chemistry is slower than molecular mixing, the reaction zone is close to the instantaneous stoichiometric surface, defined as $Z(\boldsymbol{x}, t) = Z_{st}$. This surface moves relative to the laboratory reference frame. Gibson (1968) points out that the velocity of a point fixed on an isoscalar surface of a conserved scalar can be given as

$$\boldsymbol{u}_Z = \boldsymbol{u} - \frac{D\nabla^2 Z}{|\nabla Z|}\boldsymbol{i}_Z = \boldsymbol{u} - D\nabla^2 Z \frac{\nabla Z}{|\nabla Z|^2}. \tag{3.1}$$

Here $\boldsymbol{u}$ is the fluid velocity and $\boldsymbol{i}_Z$ is the unit vector in the direction of the local mixture fraction gradient. Equation (3.1) states that the point in question moves due to both the convection of the flow field and the molecular diffusion of the scalar ('diffusion velocity').

Since the stoichiometric surface is an isoscalar surface of a conserved scalar, (3.1) can be used to compute the instantaneous velocity of any point on this surface. This makes it possible to track points on the stoichiometric surface and to examine the fields as they would appear in the frame of reference of an observer fixed to a point on this surface (Mell *et al.* 1994). To emphasize the difference between fluid particles and points on the stoichiometric surface, this study refers to the latter as 'flame elements', and the procedure of tracking them via (3.1) as 'flame element tracking'.

The tracking of flame elements was performed as follows. Initially a group of points were distributed along the stoichiometric surface. The updated positions of the flame

https://doi.org/10.1017/S0022112004001004 Published online by Cambridge University Press



FIGURE 3. Local coordinate systems used in flamelet modeling. Point O is fixed on the stoichiometric surface.

elements can be obtained by integrating the equations of motion based on the velocity given by (3.1). The integration is initiated with a second-order Runge–Kutta scheme and proceeds by a second-order Adam–Bashforth scheme. Since the DNS data refer to the computational grid, an accurate interpolation scheme is needed to determine the velocity data between grid points. In this study fourth-order-accurate cubic spline interpolation has been implemented (Yeung & Pope 1988).

Note that the diffusion velocity (second term on the right-hand side of (3.1)) changes more rapidly in space than the mixture fraction itself and this can lead to errors in the tracking procedure. The tracking routine returns flame elements in the direction of ∇Z onto the stoichiometric surface once every few time steps to avoid possible accumulation of such errors. The validity of the tracking procedure has been investigated empirically. The results coming from flame element tracking proved to be quite insensitive to reasonable changes in the number of time steps between returning the flame elements onto the surface (Sripakagorn 2002).

Also note that for the current simulation, the contribution of the diffusion velocity in (3.1) ranges from 1% to 26% over the course of the simulation. The effect of the diffusion velocity is thus significant and the results of the flame element tracking are different from Lagrangian tracking of fluid particles.

3.2. *Flamelet modelling of non-premixed combustion*

Figure 3 shows a local coordinate system fixed to a point (point O) on the stoichiometric surface. Axes x_1 and x_2 are locally (at point O) tangential to the stoichiometric surface, the third axis x_3 is perpendicular to the surface. On the second figure the x_3-coordinate is replaced by the mixture fraction coordinate that is again perpendicular to the surface locally. The time-dependent flamelet model is based on the $x_3 - Z$ coordinate transformation. At high values of the Damköhler number, derivatives with respect to x_1, x_2 are negligible and the model equation is (Peters 1984)

$$\frac{\partial Y_i}{\partial t} = \frac{\chi}{2}\frac{\partial^2 Y_i}{\partial Z^2} + w_i. \tag{3.2}$$

Neglecting the time derivative in (3.2), the (quasi-) steady flamelet model follows:

$$0 = \frac{\chi}{2}\frac{\partial^2 Y_i}{\partial Z^2} + w_i. \tag{3.3}$$

The tracking procedure provides the entire temperature and scalar dissipation rate history of the flame elements being tracked. It is possible, therefore, to implement the time-dependent flamelet model (3.2) for each tracked flame element, provided the initial conditions for the $Y_i(Z)$ profile are available. Since the DNS is initialized with the steady flamelet model (3.3), the flamelet computations are initialized in the same way. To solve the flamelet equation for a flame element, the time series of χ_{st} was taken from the tracking procedure (Sripakagorn 2002). This study assumes that the

https://doi.org/10.1017/S0022112004001004 Published online by Cambridge University Press

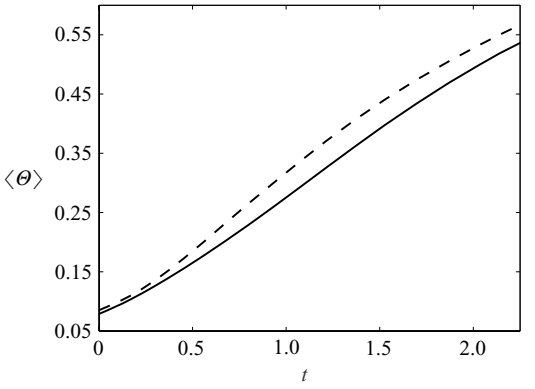


FIGURE 4. The time evolution of the average temperature. Full line: the volume-averaged temperature ($\langle\Theta\rangle$), dashed line: equilibrium chemistry prediction.

scalar dissipation rate appearing in (3.2)–(3.3) can be modelled using

$$\left.\begin{aligned}\chi(Z) &= \chi_{st} F(Z),\\ F(Z) &= \exp[-2(\mathrm{erf}^{-1}(2Z-1)^2)].\end{aligned}\right\} \tag{3.4}$$

The validity of (3.4) is discussed in Sripakagorn (2002).

According to (3.2)–(3.3), the temperature at a point on the stoichiometric surface evolves under the influence of its own scalar dissipation rate; neighbouring points on the surface have no direct influence on its temperature. Even the closest neighbours extinguish and reignite as isolated counterflows ('independent flamelets'). The main goal of the present study is the investigation of the interaction between the flamelets, i.e. the study of the thermal coupling between an extinguished flame element and its hot environment ('interacting flamelets') (Sripakagorn, Kosály & Pitsch 2000, 2001; Pitsch, Cha & Fedotov 2002).

4. Results and discussion

4.1. *Local extinction and reignition in the simulated flame*

Figure 4 shows the average temperature, $\langle\Theta\rangle$, as evaluated from the DNS data and its equilibrium chemistry prediction versus time. The temperature has been initialized with the steady flamelet solution. The two curves increase with nearly identical slopes; the simulated flame burns vigorously in a near equilibrium condition. More localized information, however, illustrates the presence of local extinction and reignition.

Figure 5 exhibits the average temperature conditioned on the stoichiometric mixture fraction ($\langle\Theta|Z_{st}\rangle \equiv \langle\Theta_{st}\rangle$) as computed from the DNS data (full line) and its steady flamelet prediction (dashed line).

Note that the dashed line was computed from (3.3), (3.4) with χ_{st} replaced by its instantaneous average. This approximation is equivalent to the quasi-steady CMC model (Bilger 1993) and represents the data correctly in the absence of extinction and reignition (Mell *et al.* 1994). Figure 5 represents extinction and reignition as an initial deviation from steady flamelet (quasi-steady CMC) behaviour followed by a gradual return to it.

Figure 6 illustrates further chronological details of extinction and reignition at stoichiometric mixture by showing Eulerian data in the (Θ_{st}, χ_{st})-plane. The solid

https://doi.org/10.1017/S0022112004001004 Published online by Cambridge University Press

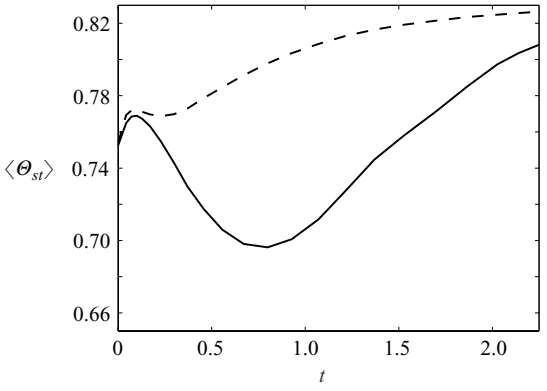


FIGURE 5. The time evolution of the average temperature conditioned on the stoichiometric mixture. Full line: $\langle \Theta | Z_{st} \rangle \equiv \langle \Theta_{st} \rangle$, dashed line: steady flamelet prediction with the fluctuations of χ_{st} neglected, i.e. (3.3), (3.4) with χ_{st} replaced by $\langle \chi_{st} \rangle$.

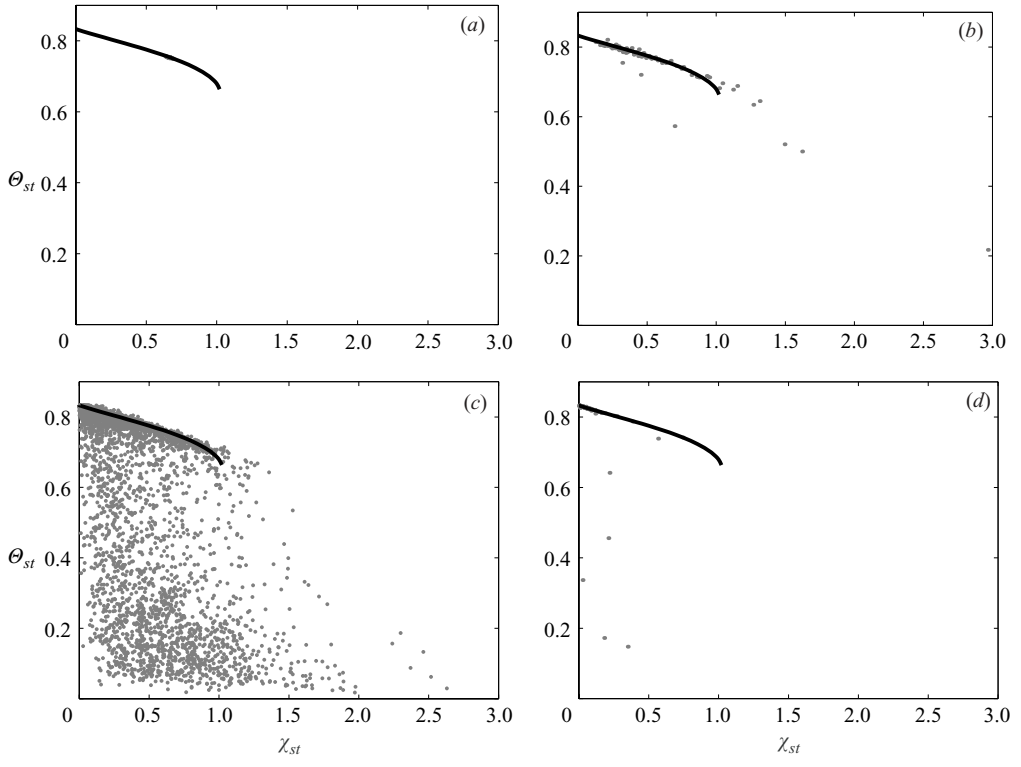


FIGURE 6. Extinction and reignition behaviour at stoichiometric mixture. Full line: burning solution of the steady-flamelet equation. The grey dots represent the normalized temperature of 8000 Eulerian data points. (*a*) $t = 0$, (*b*) $t = 0.225$, (c) $t = 0.80$, (*d*) $t = 2.03$.

line indicates the burning branch of the steady flamelet solution. The temperature was initialized with the steady flamelet solution (figure 6*a*). Early in the simulation (figure 6*b*), the flame burns vigorously, and the temperature stays close to the steady flamelet solution. In the midst of vigorous burning, the presence of local extinction

https://doi.org/10.1017/S0022112004001004 Published online by Cambridge University Press

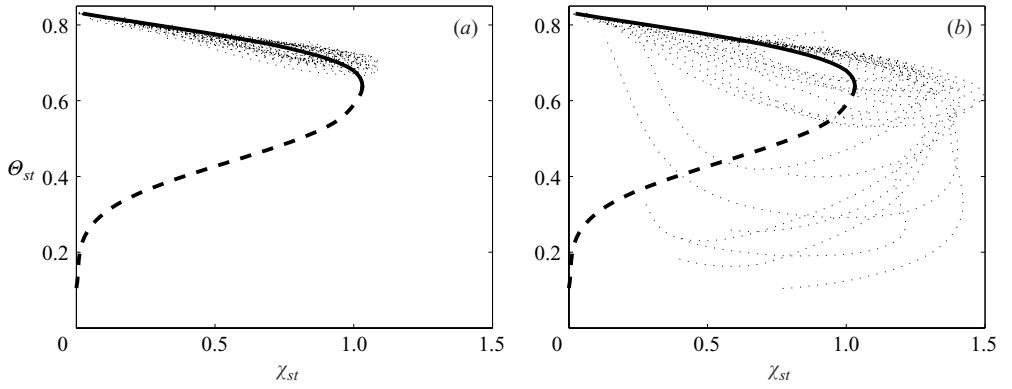


FIGURE 7. Tracked flame element trajectories in the (Θ_{st}, χ_{st})-plane ($t = 0$–1.0). (*a*) $\chi_{\max}/\chi_q < 1.1$, (*b*) $\chi_{\max}/\chi_q > 1.1$. The steady burning and unsteady branch of the steady flamelet solution are overlayed as full and dashed lines respectively.

creates strong local non-burning as evidenced by the bimodality of the temperature (figure 6*c*). By the end of the simulation, the temperature values return to the burning solutions of the steady flamelet equation, and the flame reignites (figure 6*d*).

4.2. *Extinction and reignition near to the stoichiometric surface*

The results shown in figure 6 raise questions. How does extinction happen; how does a point actually respond to the fluctuations of χ_{st} over χ_q; and what is the mechanism behind the apparent reignition of the flame?

Figure 7 employs the technique of flame element tracking to examine the response of flame elements to fluctuations in χ_{st}. The figure shows flame element trajectories in the (Θ_{st}, χ_{st})-plane. The elements were tracked over the interval $t = 0$–1.0. In figure 7, the steady flamelet solution is indicated as a full line and continued in the middle, unstable branch by a dashed line. Since the simulation was initialized with the steady flamelet solution, initially all flame elements were fully burning. The flame elements in figure 7(*a*) are associated with χ_{st} values that barely exceed χ_q. Accordingly, the trajectories in figure 7(*a*) stay close to the steady burning branch.

Figure 7(*b*) illustrates that the flame elements, whose scalar dissipation rate becomes larger than χ_q, undergo extinction. Due to the subsequent general decrease of the values of the scalar dissipation rate (figure 1), the extinguished elements are later carried back into the $\chi_{st} < \chi_q$ region where they gradually reignite. In the present results, the extinction events are mainly caused by excessive heat losses when $\chi_{st} > \chi_q$. This mode of extinction will be the focus of the present study. Regarding another, much less probable, mode of extinction, refer to Sripakagorn (2002).

Figure 7 indicates that $\chi_{st} > \chi_q$ events create extinguished regions that contribute to the many non-burning (cold) points seen in figure 6(*c*). To study in more detail how the non-burning points have been created, figure 8 shows the time evolution of the probability density function (p.d.f.) of χ_{st} and Θ_{st} obtained from the Eulerian data using a bin width of $\Delta Z = 0.015$. Look first at the p.d.f. of χ_{st} in figure 8(*a*). As an extension to figure 1, it illustrates that the initial narrow band of χ_{st} regions extends rapidly toward large and small values of this quantity. The fluctuations of χ_{st} extend well beyond the extinction value of the scalar dissipation rate ($\chi_q = 1.04$).

https://doi.org/10.1017/S0022112004001004 Published online by Cambridge University Press

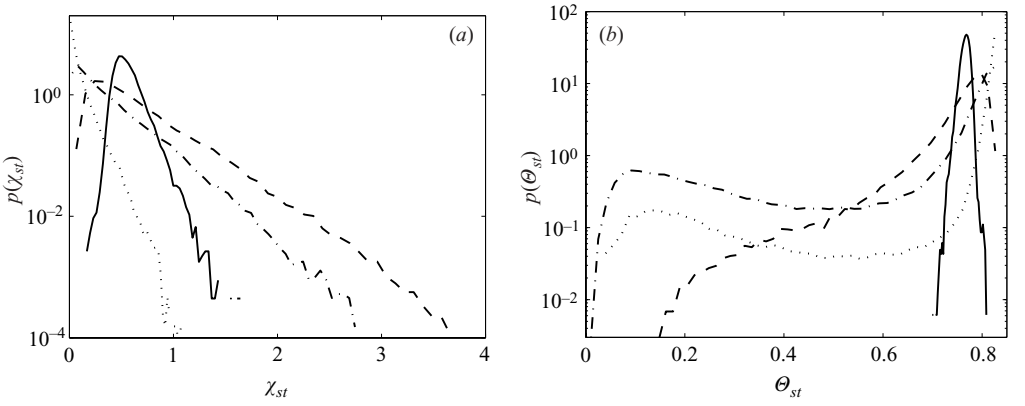


FIGURE 8. The probability density function (p.d.f.) of (*a*) the scalar dissipation rate and (*b*) the temperature at stoichiometric mixture. The data refer to Eulerian data at $t = 0.04$: full line, $t = 0.225$: dashed line, $t = 0.80$: dash-dot, and $t = 2.0$: dotted line.

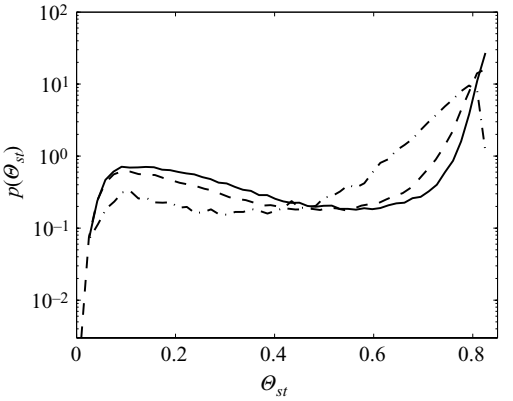


FIGURE 9. The Eulerian probability density function (p.d.f.) of the temperature at stoichiometric mixture for different values of β ($\beta = 4$: dashed line, $\beta = 2$: dash-dot, $\beta = 6$: full line). The extinction value χ_q is identical for the three cases. The data refer to $t = 0.80$. The dashed line is identical to the dashed-dot line in figure 8(*b*).

Figure 8(*b*) shows the corresponding evolution of the p.d.f. of Θ_{st}, $p(\Theta_{st})$. The initial p.d.f. describes full burning at high temperature. The p.d.f. rapidly develops a long tail at low temperatures during $t = 0$–0.80. This bimodality of $p(\Theta_{st})$ suggests that the stoichiometric region, associated with low temperatures, increases relative to the region associated with higher temperatures. Afterwards, reignition brings the temperature back to the burning condition, and the low-temperature tail subsides.

The physical reasons leading to the bimodality of $p(\Theta_{st})$ can be explained. Due to fluctuations of χ_{st} ($\chi_{st} > \chi_q$) extinguished regions are created (see figure 7). An extinction event converts a hot region into a cold one. Since there is a time lag between extinction and subsequent reignition (see discussions at the end of § 4.3.3) the extinguished regions accumulate in time. Extinction and its accumulation explains the formation of the low-temperature tail of the p.d.f.

The Zeldovich number value used in this study ($\beta = 4$) was chosen as a compromise between more realistic values and the resolution requirements related to flame element tracking. Figure 9 demonstrates the influence of the Zeldovich number on the results

https://doi.org/10.1017/S0022112004001004 Published online by Cambridge University Press

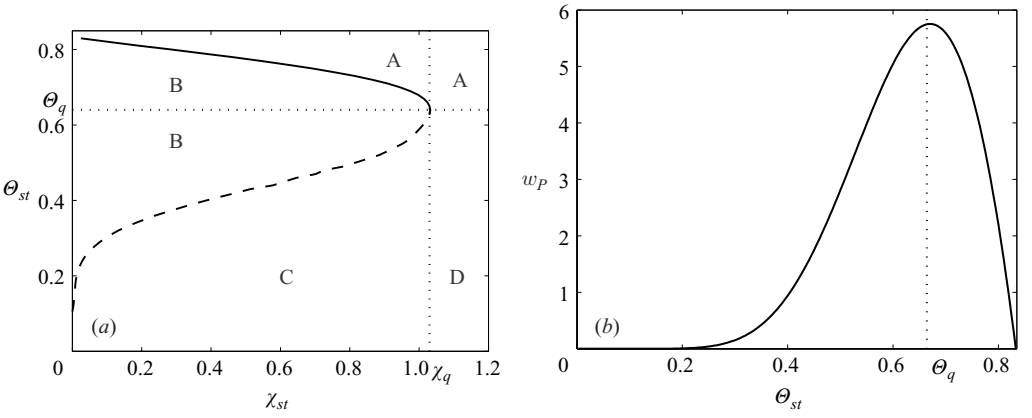


FIGURE 10. (*a*) The S-curve representing the solution of the steady flamelet equation under the present set of thermo-chemistry parameters. The burning branch is the full line followed by the unstable branch shown as a dashed line. The non-burning branch is very close to zero temperature value and cannot be seen. The regions A, B, C and D will be discussed in § 4.3.1. (*b*) The reaction rate of the product versus the non-dimensional temperature at stoichiometric mixture fraction. The vertical dotted line is at $\Theta(Z_{st}, \chi_{st} = \chi_q) \equiv \Theta_q = 0.65$ where the reaction rate is at the maximum.

shown in figure 8(*b*). In this figure the p.d.f. of Θ_{st} is plotted at $t = 0.8$ for different values of β. The figure shows that larger values of β lead to stronger bimodality in the p.d.f. of the temperature. The results for $\beta = 4$ are qualitatively similar to those at larger Zeldovich number ($\beta = 6$), while the data referring to $\beta = 2$ exhibit a broad plateau of the p.d.f. at low temperature with minimal bimodality.

Before turning to the discussion of the different scenarios of reignition, the distinction between burning and extinguished flame elements should be quantified. Figure 10(*a*) shows the burning solution (full line) of the steady flamelet solution continued into the unstable solution (dashed line), using the chemistry parameters given in table 2. The horizontal dotted line indicates the smallest possible temperature belonging to the burning solution ($\Theta_q = 0.65$); the vertical dotted line is at $\chi_q = 1.04$. This paper refers to flame elements with temperature above Θ_q as burning elements; the ones with temperature below that value are considered as being extinguished. An element has reignited when its temperature changes from $\Theta_{st} < \Theta_q$ to $\Theta_{st} > \Theta_q$.

In figure 10(*b*) the reaction rate of the product is plotted against the temperature at stoichiometric mixture. The vertical dotted line is at $\Theta_{st} = \Theta_q$. The reaction rate of the product has a maximum ($w_{P,\max} = 5.8$) at this value.

4.3. *Reignition scenarios*

This section discusses the behaviour of flame elements whose history has been followed from initialization via flame element tracking. The initial conditions are known from the initialization of the DNS; the time history of Θ_{st} and χ_{st} are continuously recorded for each flame element. With this information the time-dependent flamelet equation can be solved for the tracked flame elements and the temporal development predicted by the flamelet equation can be compared with the DNS data. Using flame element tracking data, coupled with the three-dimensional flame structure, three different scenarios of reignition are identified.

https://doi.org/10.1017/S0022112004001004 Published online by Cambridge University Press

In the first scenario, the excursion of the scalar dissipation rate fluctuation above χ_q is relatively small and quick, such that it does not lead to very low temperatures. The flame element is able to return to full burning without substantial interaction with the surroundings. The time-dependent flamelet model predicts the entire time history of the temperature fluctuation quite accurately. This study refers to this case as the independent flamelet scenario.

When the excursion of the scalar dissipation rate fluctuation above χ_q is large and lasts for a long time, the temperature of the flame element drops significantly. The element cannot be reignited without the influence of the hot environment. Since the time-dependent flamelet model does not account for this influence, it is able to predict extinction but fails to describe reignition. This study finds that the interaction between hot environment and cold elements may take place in two basic ways. The heat may approach the extinguished flame element from its neighbours along the stoichiometric surface via premixed flame propagation. The other possibility is that the heat flux is due to hot surfaces being swept toward the cold region by turbulent convection. These two avenues to reignition are termed in this paper the edge flame propagation and the engulfment scenario, respectively. The latter scenario corresponds to the 'flame–flame interaction' in the recent paper of Hewson & Kerstein (2002).

To distinguish between different scenarios this study monitors the local, instantaneous behaviour of the following quantities:

$$\left.\begin{aligned} &\text{normalized flame index,} \quad G_s = \frac{\nabla Y_F \cdot \nabla Y_O}{|\nabla Y_F||\nabla Y_O|}, \\ &\text{lateral diffusion term,} \quad i_p = D\left(\frac{\partial^2 \Theta}{\partial x_1^2} + \frac{\partial^2 \Theta}{\partial x_2^2}\right), \\ &\text{normal diffusion term,} \quad i_n = D\frac{\partial^2 \Theta}{\partial x_3^2}. \end{aligned}\right\} \tag{4.1}$$

The above quantities are computed in the local (moving) coordinate system shown in figure 3 as part of the tracking procedure. They are evaluated at point O, the origin of the coordinate system. The flame index G_s is used as a diagnostic tool to identify the presence of premixed burning (see Favier & Vervisch 2001; Sripakagorn 2002). In a burning or frozen diffusion flame, $G_s = -1$, while in partially premixed combustion $G_s > -1$. The terms i_p and i_n characterize the heat conduction per unit time in the (x_1, x_2)-plane and in the x_3-direction, respectively. In a burning flame element, i_p is zero and i_n is negative. If i_p is positive, heat is conducted toward the flame element in the direction parallel to the stoichiometric surface; positive i_n means that heat is conducted toward the flame element along the direction normal to the stoichiometric surface.

The next three sections (§§ 4.3.1–4.3.3) discuss examples of originally burning flame elements that extinguish and then reignite by way of the different scenarios. Individual time histories will be shown together with instantaneous spatial behaviour, to illustrate the idea of diagnosing the different scenarios from the values of G_s, i_p, and i_n at the time of reignition. The summary of findings that relate the diagnostics to different scenarios are in table 3.

4.3.1. *Independent flamelet scenario*

Figure 11 shows a typical case for which a quick transient in χ_{st} over the extinction threshold results in a minor decrease and subsequent increase in temperature that

https://doi.org/10.1017/S0022112004001004 Published online by Cambridge University Press

Diagnostics			Process
$i_n < 0$	$i_p \simeq 0$	$G_s = -1$	Burning
$i_n \simeq 0$	$i_p \simeq 0$	$G_s = -1$	Extinguished (non-burning)
$i_n < 0$	$i_p \simeq 0$	$G_s < -0.8$	Reignition: independent flamelet
$i_n < 0$	$i_p > 0$	$G_s > -1$	Reignition: edge flame propagation
$i_n > 0$	$i_p \simeq 0$	$G_s > -1$	Reignition: engulfment
$i_n > 0$	$i_p > 0$	$G_s > -1$	Reignition: engulfment

TABLE 3. Characteristic signs/values of the (4.1) diagnostics and the physical processes they characterize.

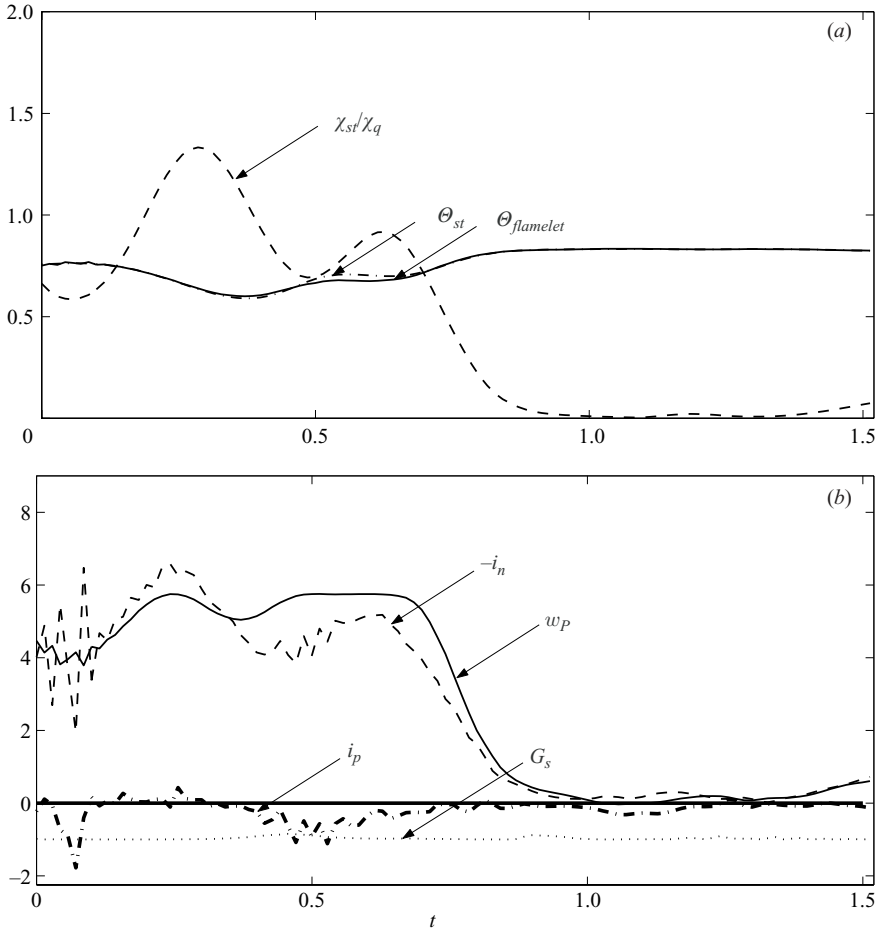


FIGURE 11. Independent flamelet reignition. (*a*) The time evolution of χ_{st}/χ_q (dashed line), Θ_{st} from DNS (full line) and time-dependent flamelet prediction (dash-dot). (*b*) The time evolution of G_s (dots), i_p (bold dash-dot), $-i_n$ (dashed), and reaction rate w_P (full line).

is well-predicted by the time-dependent flamelet model (3.2). Figure 11(*a*) compares the time evolution of the temperature obtained from the DNS to the corresponding flamelet calculation and shows the evolution of χ_{st}/χ_q. In figure 11(*b*) the quantities defined in (4.1) and the reaction rate of the product are plotted. The results show that

https://doi.org/10.1017/S0022112004001004 Published online by Cambridge University Press

at $t \simeq 0.4$, when reignition takes place, (i) there is no appreciable interaction with the neighbouring flame elements along the stoichiometric surface ($i_p \simeq 0$), (ii) the heat flux is predominantly normal to the hot stoichiometric surface, pointing away from it ($i_n < 0$), and (iii) there is no premixed combustion involved ($G_s \simeq -1$).

For the discussion of this reignition scenario we refer to figure 10(*a*). It is a known property of the time-dependent flamelet equation that flame elements from regions B or C will be attracted to the burning or non-burning solutions, respectively (Pitsch & Fedotov 2001). Figure 7(*b*) shows that extinguishing–reigniting flame elements move from area A to areas D, C and B in this order. Once the flame element is in B, and its temperature is below Θ_q, the time-dependent flamelet model predicts reignition via an independent flamelet. The flamelet equation (3.2) does not describe, however, the transfer from C to B, unless the scalar dissipation rate of the element decreases sufficiently fast, so that there is not enough time for a large temperature drop and the flame element can enter B by crossing the dashed line moving in the south-west direction (Pitsch & Fedotov 2001). Note that at higher values of β the unstable branch in figure 10(*a*) (dashed line) would be more horizontal, and the part of B below the $\Theta_q = 0.65$ dotted line would become smaller (Pitsch & Fedotov 2001). The expectation, therefore, is that the present use of a relatively low Zeldovich number leads to an amplification of the importance of the independent flamelet scenario.

4.3.2. *Reignition due to propagating edge flames*

Figure 12 shows a case for which the scalar dissipation rate is larger than χ_q for an extended period of time. The data indicate reignition while the time-dependent flamelet model predicts complete extinction (figure 12*a*). Figure 12(*b*) again shows the quantities defined in (4.1) and the reaction rate of the product. It will be argued that reignition is due to lateral thermal interaction along the stoichiometric surface. The study of flame structure indicates that the thermal interaction acts via propagating edge (triple) flames.

Figure 12 illustrates the process of extinction and reignition of the flame element. Immediately after initialization ($t = 0$–0.2) the flame element is burning in the quasi-steady mode. The initial increase of χ_{st} is accompanied by the increase of the reaction rate and the slow decrease of the temperature. During $t = 0.2$–0.5 the flame extinguishes; the reaction rate decreases to almost zero. The temperature stays low until $t \simeq 0.9$, when it starts increasing. At this time, i_p is consistently positive, showing that the temperature increase is due to heat flux between the extinguished element and the neighbouring hot regions along the stoichiometric surface. Once the temperature becomes sufficiently high ($t \simeq 1.25$), the reaction rate term becomes significantly larger than the heat losses characterized by i_n, and the flame element reignites. Examination of the evolution of G_s in figure 12(*b*) shows that premixed combustion plays an important role. In the $t = 0$–1.0 interval, the originally burning flame element becomes extinguished and gradually frozen; premixed combustion is negligible, $G_s = -1$. After extinction, fuel and oxidant mix without reaction leading to premixed combustion when the triple flame burns into the premixture ($t = 1$–1.5, $G_s > -1$). After reignition ($t \simeq 1.5$), the premixture is consumed; a diffusion flame persists ($G_s = -1$, $i_p = 0$). Throughout the process $i_n < 0$, the net radial heat flux points away from the surface. In the time region when the flame element is approximately frozen, i_n is still negative but its absolute value is small.

Figure 13 shows contour plots of scalars along two-dimensional cuts of the computational volume. The full lines are contour lines of Θ between 0.6 and 0.8

https://doi.org/10.1017/S0022112004001004 Published online by Cambridge University Press

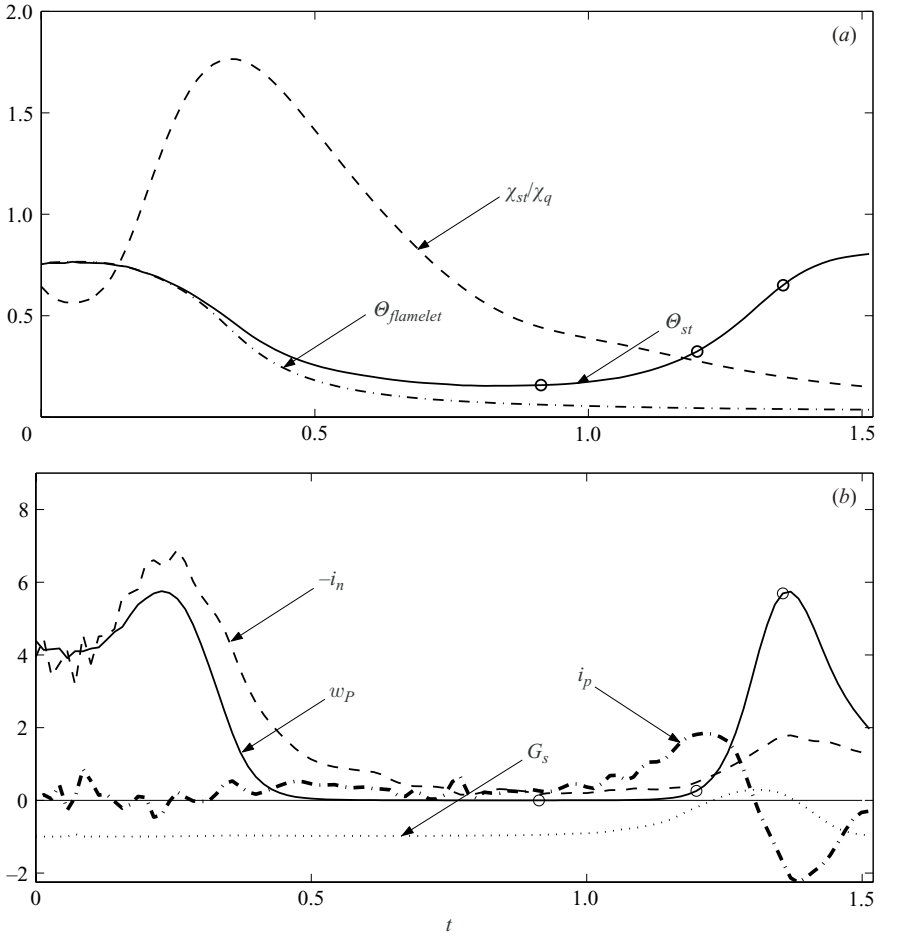


FIGURE 12. Reignition via edge flame propagation. (*a*) The time evolution of χ_{st}/χ_q (dashed line), Θ_{st} from DNS (full line) and time-dependent flamelet prediction (dash-dot). (*b*) The time evolution of G_s (dots), i_p (bold dash-dot), $-i_n$ (dashed), and reaction rate w_P (full line). Circles indicate the times corresponding to the three-plot sequence in figure 13.

at steps of 0.1. The bold full line corresponds to $\Theta = 0.5$; this is the temperature where the stoichiometric reaction rate reaches half of its maximum value. Most of the chemical reactions take place in the area enclosed by the bold full lines. The dashed line indicates the local stoichiometric surface. The circle at the centre of the frame represents the flame element discussed in figure 12. The plane shown in the figure was chosen to be tangential to the stoichiometric surface at the instantaneous position of the flame element. To verify that the plane is indeed tangential, each figure includes three dashed lines corresponding to the $Z = 0.48, 0.50$, and 0.52 isocontours. In the vicinity of the flame element the dashed lines converge as expected.

Figure 13(*a*) captures the moment just before the temperature of the flame element starts to increase (cf. figure 12*a*); the flame element is extinguished in a cold region. Shortly thereafter, reignition starts due to heat flux approaching from above (figure 13*b*). In principle, the flame approaching the tracked flame element shown in figure 13 could also be attributed to relative convection between a hot surface and

https://doi.org/10.1017/S0022112004001004 Published online by Cambridge University Press

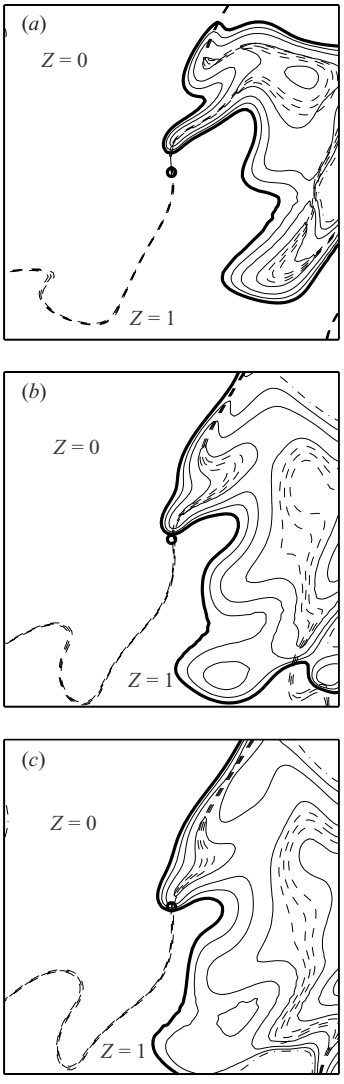


FIGURE 13. Reignition sequence (edge flame propagation). The temperature contours $\Theta = 0.5$ are in bold full lines, $\Theta = 0.6, 0.7, 0.8$ are thinner. $\Theta = 0.5$ is where the reaction rate drops to half of its peak value for $Z = 0.5$. Most of the chemical reaction takes place within this contour. The flame element is indicated by a circle at the centre of the frame. The plane shown in the figures was chosen to be perpendicular to the stoichiometric surface at the position of the flame element. The $Z = 0.48, 0.50, 0.52$ isocontours are represented by dashed lines. In the vicinity of the flame element the dashed lines converge as expected. (*a*) $t = 0.93$, (*b*) $t = 1.21$, (*c*) $t = 1.37$.

the extinguished element. However, since the most compressive strain tends to be locally perpendicular to the stoichiometric surface and the extensive strain stretches the surface, rather than compresses it (Ashurst *et al.* 1987), this is generally not the case.

Returning to the discussion of the lateral diffusion term i_p, figure 12(*b*) demonstrates that after exhibiting a positive peak at the start of reignition, i_p becomes negative

https://doi.org/10.1017/S0022112004001004 Published online by Cambridge University Press

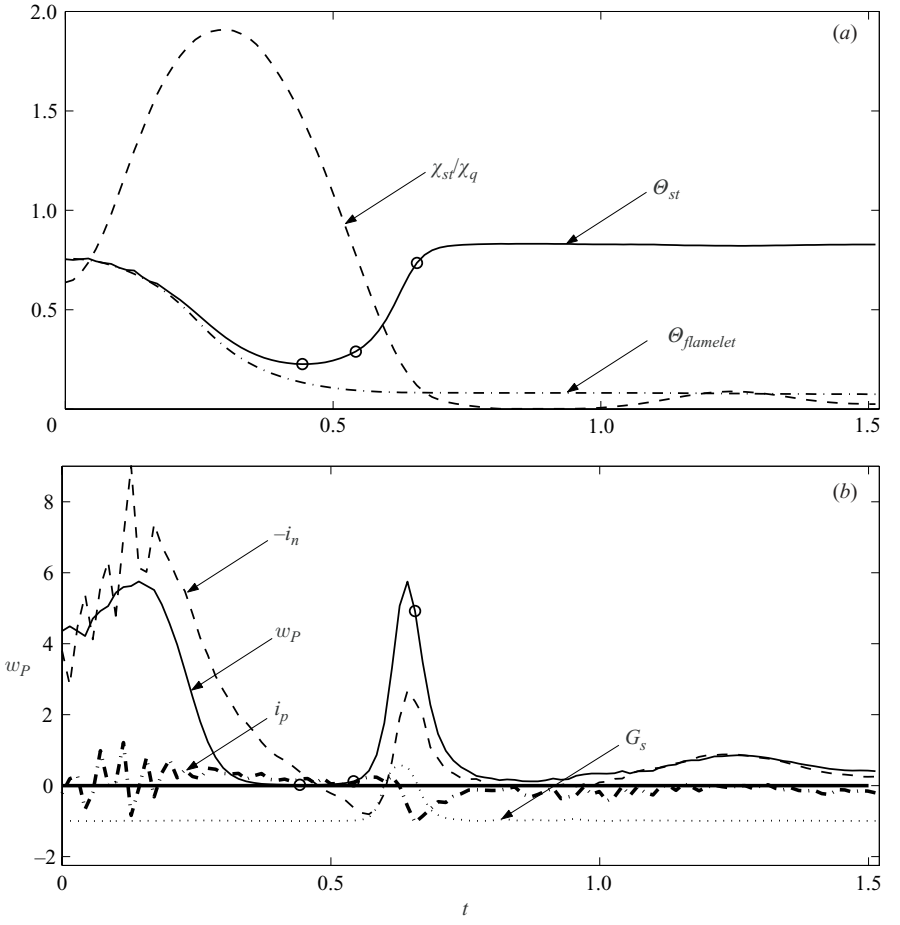


FIGURE 14. Reignition via perpendicular engulfment. (*a*) The time evolution of χ_{st}/χ_q (dashed line), Θ_{st} from DNS (full line) and time-dependent flamelet prediction (dash-dot). (*b*) The time evolution of G_s (dots), i_p (bold dash-dot), $-i_n$ (dashed), and reaction rate w_P (full line). Circles indicate the times corresponding to the three-plot sequence in figure 15.

before becoming negligible. This can be understood, since after its reignition due to a triple flame approaching it from one side, the flame element is still adjacent to an extinguished region on the other side (figure 13*c*). The negative value of i_p is due to the diffusion of heat from the reignited element toward the extinguished neighbours.

4.3.3. *Reignition due to engulfment by the hot neighbourhood*

Figure 14 (*a*, *b*) again shows time histories related to the extinction and subsequent reignition of a flame element. First, focus on figure 14(*b*). Before reignition, there is not much difference between this figure and figure 12(*b*): even the normal diffusion term, i_n, behaves similarly to before ($i_n < 0$). However, in contrast to the earlier case, the strong increase of the reaction rate from a zero value is preceded by a positive peak of i_n (figure 14*b*, $t \simeq 0.5$). A comparison of i_n and i_p suggests that the heat flux causing the reignition comes primarily from the perpendicular direction of the stoichiometric surface rather than from adjacent areas within the surface. Indeed, at the time of reignition, i_p stays small. It becomes large and negative after reignition,

https://doi.org/10.1017/S0022112004001004 Published online by Cambridge University Press

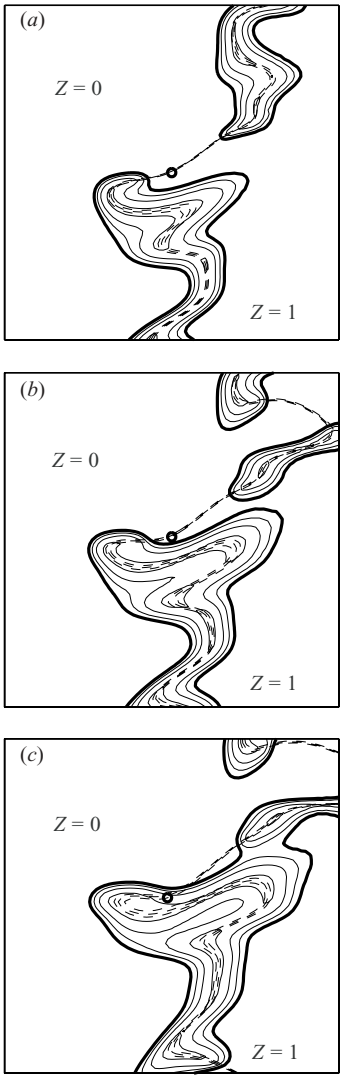


FIGURE 15. Reignition sequence (perpendicular engulfment). See the caption to figure 13. (*a*) $t = 0.46$, (*b*) $t = 0.56$, (*c*) $t = 0.67$.

when the reignited kernel initiates an edge flame burning into the adjacent region that is still cold. Figure 15 provides more detailed information and demonstrates that the extinguished flame element is indeed reignited via engulfment by a neighbouring hot flame parcel. Since the heat flux points toward the flame element on the stoichiometric surface, the normal diffusion term i_n is necessarily positive when reignition starts.

There are many cases, where, at the time of reignition, both i_p and i_n are positive. In such cases, reignition may take place via perpendicular engulfment accompanied by simultaneous edge flame propagation along the stoichiometric surface or via flame engulfment but in an oblique direction. Figure 16 displays such cases. Figure 16(a, b) shows the temperature and scalar dissipation rate of the two reigniting elements. At the time of reignition, both i_p and i_n, shown figure 16(c, d), are positive, suggesting heat diffusion into the flame element from both lateral and normal directions. Although

https://doi.org/10.1017/S0022112004001004 Published online by Cambridge University Press

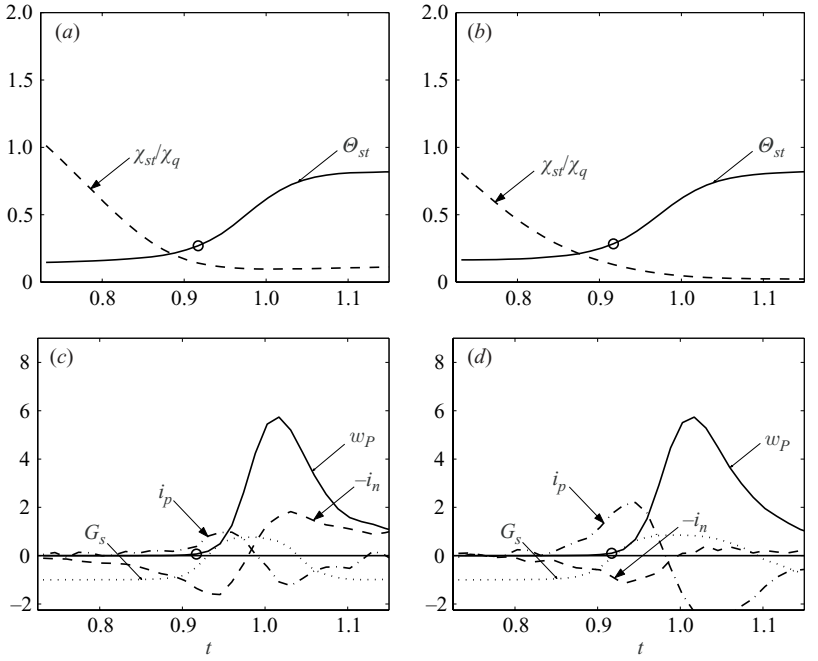


FIGURE 16. Reignition due to a combination of perpendicular engulfment and edge flame (flame element 1) and engulfment from an obligue direction (flame element 2). (a, b) The time evolution of χ_{st}/χ_q (dots) and Θ_{st} from DNS (solid line). (c, d) The time evolution of G_s (dots), i_p (dash-dot), $-i_n$ (dashed), and reaction rate w_P (solid line). Circles indicate the times corresponding to figure 17.

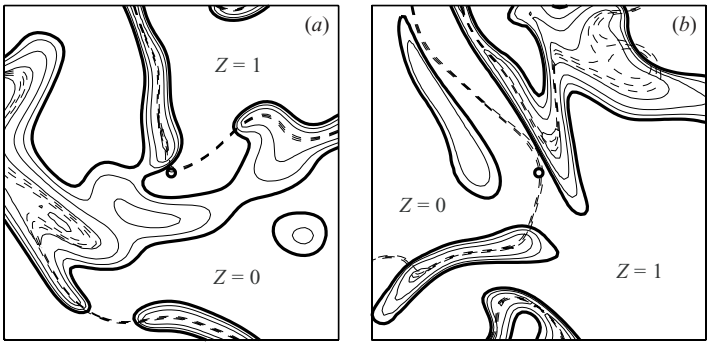


FIGURE 17. (a) Reignition due to a combination between perpendicular engulfment and edge flame propagation: flame element 1 at $t = 0.93$ (b) Reignition due to engulfment from an obligue direction: flame element 2 at $t = 0.93$. See caption to figure 13.

the two time histories in figure 16(b) look quite similar, figure 17 shows the difference in the flame structures. Flame element 1 is approached both by an edge flame (from the top) and an engulfing region (from the left). The second flame element, however, is engulfed by the flame region (from the top right) without any edge flame in the vicinity. It turns out that engulfment from an oblique direction may lead to a positive peak in i_p even in the absence of a lateral premixed flame front. Examination of a large number of flame elements suggests that 'oblique engulfment' is more prevalent than the true mixed scenario illustrated by flame element 1.

https://doi.org/10.1017/S0022112004001004 Published online by Cambridge University Press

In the case of element 2, after it has been reignited by engulfment from an oblique direction an edge flame may be formed and reignite the rest of the cold region via a mixed scenario similar to the situation for flame element 1. Figures 14–17 demonstrate that reignition via engulfment covers a wide variety of possibilities including a contribution by edge flames.

Let us discuss finally the relative time scales of extinction and reignition. In the independent flamelet scenario, reignition follows immediately once χ_{st} drops below χ_q. Figures 12, 14, and 16 show, however, that in the edge flame propagation and engulfment cases reignition occurs well after extinction has been completed. In these scenarios, reignition cannot start before an influx of heat from the hot environment reaches the cold region. Reignition at a particular cold location involves the arrival of a propagating edge flame and/or an engulfing flame front. It will be shown in § 4.4 that the independent flamelet plays only a minor role in reignition. In this study, therefore, reignition is typically takes longer than extinction.

4.3.4. *Eulerian vs. tracking data*

Figures 5 and 8 provide statistical information on extinction and reignition near to the stoichiometric surface. The information in figure 6 and the discussion in §§ 4.3.1–4.3.3 are not statistical, they refer to individual flame elements. The next goal is to provide statistical information regarding the reignition scenarios. For this purpose, flame element tracking is employed to determine the relative contribution of the different scenarios to the reignition illustrated in figures 5 and 8. Note, however, that flame element tracking refers to the stoichiometric surface, while the conditional average shown in figure 5 and the conditional p.d.f.s seen in figure 8 both refer to Eulerian grid points within the finite instantaneous volume between the surfaces $Z_{st} \pm \Delta Z$ ($\Delta Z = 0.015$). To determine the role different scenarios play in the behaviour shown in figure 5 and figure 8, we have to select groups of flame elements such that the instantaneous tracking results will provide information on the Eulerian grid points in the instantaneous volume.

The most plausible idea is to select at $t = 0$ a group of flame elements that are approximately uniformly distributed along the stoichiometric surface and track them for $t > 0$. The hope is that the results referring to the selected flame elements will characterize well what is happening in the finite instantaneous volume. To investigate the matter, we selected randomly a group of grid points in the volume at a time and projected them along the ∇Z-direction onto the stoichiometric surface and evaluated the p.d.f.s of χ_{st} and Θ_{st} from both the grid point data and from the ensemble of the selected flame elements. Figure 18(a, b) demonstrates that the grid point p.d.f.s (circles) approximately coincide with the p.d.f.s evaluated from the flame elements (crosses). This means that, at the time of selection, the ensemble of flame elements represents correctly the ensemble of grid points within the instantaneous volume. At later times, however, the volume changes its shape and it is not certain that the flame elements selected at a time will continue to be representative of the grid points at a later time. Indeed, figures 18(c) and 18(d) demonstrate marked differences between the circles and the crosses. This difference is not related to poor statistics as the results are proven insensitive to the increase in the number of initial flame elements (not shown). The deviation between the dots and the crosses is a physical effect caused by the continuous change of the shape and size of the volume of the stoichiometric mixture defined by the ΔZ half-width. To characterize this volume with tracked data it is necessary to reinitialize the tracked ensemble from time to time.

https://doi.org/10.1017/S0022112004001004 Published online by Cambridge University Press

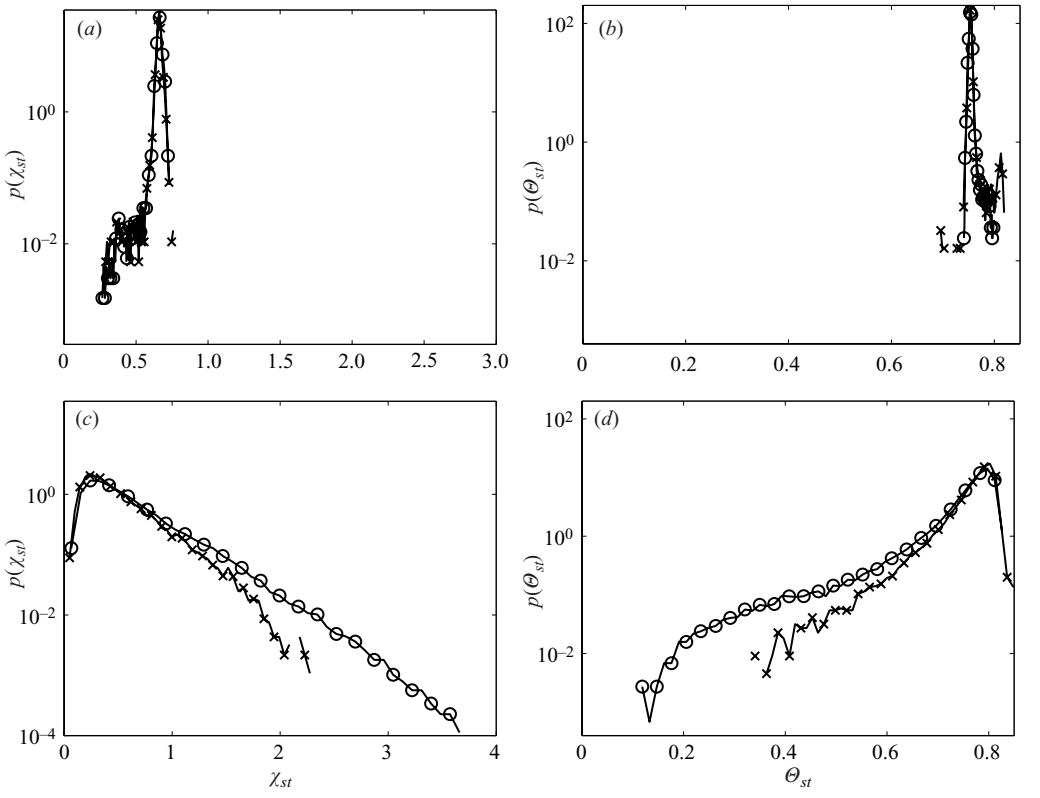


FIGURE 18. The probability density function (p.d.f.) of the scalar dissipation rate (a, c) and the temperature (b, d) at stoichiometric mixture. The circles indicate Eulerian data, the crosses refer to tracked flame elements initiated at $t = 0$. (a, b) $t = 0$, (c, d) $t = 0.225$.

4.4. *Relative importance of the reignition scenarios*

In §4.3 different scenarios of reignition are identified via the diagnostics i_p, i_n, and G_s. To determine the relative importance of the scenarios the scope of this study is to be extended in two ways. As discussed in §4.3.4, the flame element tracking must be reinitialized periodically to correctly represent the Eulerian statistics. Therefore, the first step is to determine the time interval in which the tracking results will be reinitialized. Secondly, a large number of cases need to be examined to get good statistics: the investigation of time histories one-by-one is no longer practical. To automate the diagnostic process, one has to define the time period when reignition takes place and decide when the diagnostics defined in (4.1) will be evaluated. Table 3 is also to be complemented with numerical threshold values that distinguish between the true positive values of the diagnostics and their irrelevant fluctuations. These two extensions are discussed in detail in Sripakagorn (2002). Next the main findings of that dissertation regarding this matter will be reviewed.

First, we discuss the choice of the time interval. The interval should be sufficiently small to allow the tracking ensemble to approximately characterize the grid point data in the instantaneous volume of half-width ΔZ about the stoichiometric surface, while also sufficiently large to allow the reignition process to be completed. The value used in this study is $\Delta t = 0.3$ (Sripakagorn 2002). Secondly, we consider the numerical criteria to diagnose reignition scenarios. The finding is that the diagnostics are to

https://doi.org/10.1017/S0022112004001004 Published online by Cambridge University Press

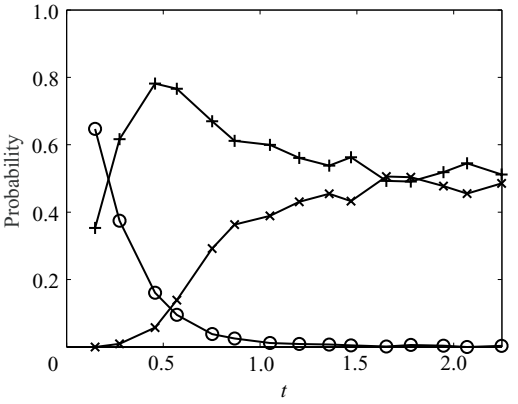


FIGURE 19. Conditional probability that if reignition takes place at time t, it will take place through a particular scenario. Circles: independent flamelet, plus signs: edge flame propagation, and crosses: engulfment.

be computed at the time when w_P surges from near zero to 0.46 ($w_{P,\max} = 5.8$). The appropriate threshold to distinguish between the true positive values of i_p and i_n and their irrelevant fluctuations turns out to be identical for both i_p and i_n and equal to the above characteristic value of w_P (0.46). The threshold of G_s employed in the categorization of independent flamelet is $G_s < -0.8$. In the rest of this section we use the above numerical values to investigate the relative importance of the reignition scenarios in our simulations.

To examine reignition, the number of flame elements that are reigniting via each of the three scenarios, in a given time interval, has been counted and divided by the total number of reigniting flame elements within the time interval. The results are plotted in figure 19. The data are shown at the centre of the time interval in which the group of flame elements has been tracked. The curves in figure 19 approximate the conditional probability that if reignition takes place at a given time, it will happen through one of the scenarios. It is apparent from figure 19 that the independent flamelet is of minor importance, except early in the simulation. The edge flame propagation scenario dominates the reignition scene early and remains important throughout the time observed. The influence of the engulfment scenario does not emerge until $t \simeq 0.5$. After this time its probability increases to about the same level as edge flame propagation.

Figure 20 provides further insight into the role different scenarios play in the reignition process. The figure shows the time evolution of extinguishing and reigniting flame elements that were tracked over $t = 0$–0.9. Choosing other time intervals leads to qualitatively similar results. Figure 20(a) indicates brief and mild extinctions followed by reignition, characteristics of the independent flamelet scenario. Such mild transients are initiated by small fluctuations of χ_{st} that are dominant before $t \simeq 0.3$ (cf. figure 1). The time histories plotted in figure 20(b,c) show cases when reignition requires the influence of the hot environment. A comparison between the time histories in figures 20(b) and 20(c) demonstrates that edge flames, typically, reignite moderately extinguished (not very cold) elements. The engulfment scenario, in contrast, reignites elements whose temperature is low, and does that relatively late in the simulations. To emphasize this point, note that average minimum temperatures in figures 20(b) and 20(c) are 0.5 and 0.26, respectively.

https://doi.org/10.1017/S0022112004001004 Published online by Cambridge University Press

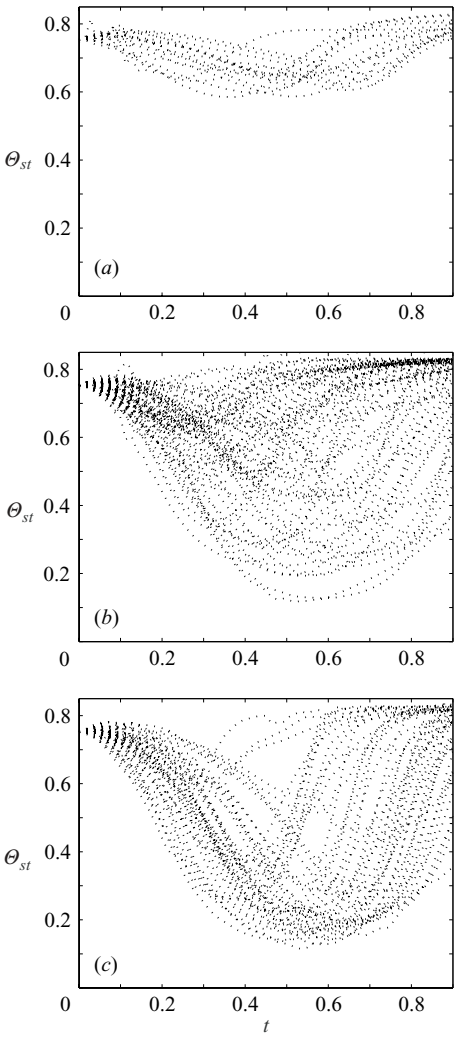


FIGURE 20. The time evolution of the temperature of tracked flame element ($t = 0$–0.9) that are associated with different reignition scenarios. (*a*) independent flamelet (17 flame elements included); (*b*) edge flame propagation (50 flame elements included); (*c*) engulfment (50 flame elements included).

To discuss the scenarios further, note that the edge flame propagation scenario is related to premixed flame propagation along a surface and will, therefore, play an important role in the reignition of laminar flames as well. The independent flamelet is not specific to turbulence either. These two scenarios are to be contrasted with the engulfment scenario, which involves the folding of the stoichiometric surface in three-dimensional space, a turbulent phenomenon. Figure 20(b, c) suggests that the premixed flame propagation is quicker than turbulent stretching and folding; reignition via the engulfment scenario is more effective but takes more time.

Figure 19 shows the conditional probability of the different reignition scenarios at a given time, but does not answer, e.g., the question of which scenario contributes the most to the reignition during the entire simulation. The probability of reignition varies over time. The scenario that is dominant when the probability of reignition is large

https://doi.org/10.1017/S0022112004001004 Published online by Cambridge University Press

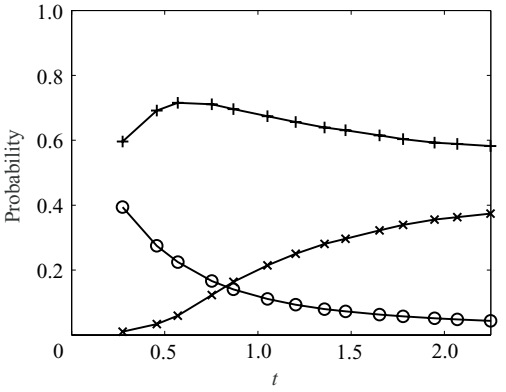


FIGURE 21. Conditional probability that if reignition takes place over (0, t) it will take place through a particular scenario. Circles: independent flamelet, plus signs: edge flame propagation, and crosses: engulfment.

has the best chance to be the most probable. This effect was included into figure 21 which shows the conditional probability that, if reignition takes place in the (0,t) interval, it will take place through one of the three scenarios. Similarly to figure 19, the contribution of the independent flamelet scenario to the total reignition picture is a mere 4% over the time interval. The engulfment scenario is more important and contributes approximately 38%. The early dominance of the edge flame propagation provides a lasting effect and its final contribution sums to 58%. In this simulated flame, the edge flame propagation is the most dominant scenario of reignition.

Finally, let us speculate about the possible consequences of using more realistic Zeldovich and Reynolds number values than considered in the present study. Figure 9 demonstrates that the temperature difference between the extinguished regions and the burning flamelets increases with the Zeldovich number. Since figure 20 shows that independent flamelet and edge flame propagation tend to reignite moderately extinguished elements, it seems plausible to expect that the importance of these two scenarios would decrease for higher Zeldovich number values. (See also the remark in the last paragraph of § 4.3.1.)

Keeping the chemistry as given in table 2, but considering stronger turbulence (larger initial Reynolds number), would result in larger fluctuations of the scalar dissipation rate and lead to more extinction. This, together with more intensive folding of the stoichiometric surface, may increase the importance of the engulfment scenario versus the other two possibilities.

Note again that the above comments on the possible influence of higher Zeldovich and Reynolds number values on the results are speculations. The clarification of these important issues requires further research. An important goal of further research will be to find out if the engulfment scenario is indeed the most dominant one in practical cases, as postulated in the work of Hewson & Kerstein (2002).

5. Concluding remarks

This study investigates local extinction and reignition in non-premixed turbulent combustion using highly resolved DNS. Initially, the entire stoichiometric surface is burning. The average temperature remains close to the equilibrium chemistry value throughout the simulation. Early in the simulation, the scalar dissipation rate exhibits

https://doi.org/10.1017/S0022112004001004 Published online by Cambridge University Press

strong fluctuations and extinguished regions appear on the stoichiometric surface (local extinction). Later in the process, the stoichiometric surface again becomes uniformly hot (reignition).

The data demonstrate that before extinction and after reignition the steady flamelet model represents correctly the simulated data (Overholt & Pope 1999). Extinction is governed by the characteristic threshold value of the scalar dissipation rate (χ_q) derived from the steady flamelet equation (Peters 1983). The average scalar dissipation rate at the stoichiometric value of the mixture fraction remains lower than the extinction threshold throughout the simulation ($\langle\chi_{st}\rangle < \chi_q$). Inspection of the fluctuations of instantaneous χ_{st} values (figure 1) demonstrate that the majority of the extinction events are caused by the fluctuations of χ_{st} over χ_q.

While the average temperature increases throughout the simulation, the average and the probability density (p.d.f.) of the temperature conditioned on the stoichiometric value of the mixture fraction provide more localized information. Extinction and reignition causes decrease and subsequent increase of the average temperature of the stoichiometric surface. Similarly, the p.d.f. of the temperature of this surface develops a strong low-temperature tail (bimodal p.d.f.) that subsides later. The time evolution of the p.d.f. of χ_{st} corroborates further the role of the fluctuations of χ_{st} in the extinction. The initial values of χ_{st} are within a rather narrow band. Soon after initialization the p.d.f. of χ_{st} extends toward small and large values of this quantity. The initial extinction is due to the p.d.f. extending well beyond the extinction limit. The bimodality of the temperature p.d.f. is related to the time lag between extinction and reignition.

The Eulerian data (averages, p.d.f.s) demonstrate extinction and reignition of the simulated flame but do not provide information on the different physical mechanisms leading to reignition. This study tracks flame elements, which are associated with individual points on the stoichiometric surface, to examine the different scenarios of reignition (Mell *et al.* 1994). The analysis of the data led to the identification of three major scenarios: the independent flamelet scenario, reignition via edge flame propagation, and reignition through engulfment by a hot neighbourhood.

Based on the analysis of individual flame element histories, diagnostic tools have been defined whose values and signs can be used to distinguish between different scenarios and investigate the reignition process. The diagnostics used in this study refer to the tracked flame element and are as follows (cf. (4.1)): the normalized flame index (G_s) that distinguishes between premixed and non-premixed combustion; and the lateral and the normal heat fluxes (i_p and i_n) that measure the heat flux toward the flame element from the direction locally parallel and perpendicular to the stoichiometric surface, respectively. The criteria used to distinguish between the different scenarios are summarized in table 3.

The results give insight into the role the different scenarios play in the reignition process. It turns out that the independent flamelet scenario serves to reignite mild extinctions initiated by small fluctuations of χ_{st}. Colder regions cannot be reignited without heat flux from the hot environment. In the edge flame propagation scenario, the edge flame reaching the cold region was shown to be a triple flame. The edge flame propagation scenario will, typically, reignite moderately extinguished elements, which means that the edge flames will reignite moderately cold regions. The engulfment scenario reignites colder regions, relatively late in the simulation.

The edge flame propagation scenario is related to locally one-dimensional premixed flame propagation and will, therefore, play an important role in the reignition of laminar flames as well. The independent flamelet scenario is not specific to

https://doi.org/10.1017/S0022112004001004 Published online by Cambridge University Press

turbulence either. These two scenarios are to be contrasted with the engulfment scenario which involves the folding of the stoichiometric surface in three-dimensional space; a turbulent phenomenon.

Regarding the importance of the different scenarios in the reignition of the simulated flame in this study, it turns out that the independent flamelet scenario is responsible only for 4% of the reignitions, while edge flame propagation and engulfment contribute to 58% and 38% of the reignitions, respectively. It can be speculated (see the end of §4.4) that at higher values of the Zeldovich and Reynolds numbers the engulfment scenario will play a larger role than in the present simulated flame. This issue, however, needs to be investigated further. An important conclusion of the present work is that flame element tracking is a viable technique that can be applied in further investigations.

The authors are indebted to Professors J. C. Kramlich and J. J. Riley at the University of Washington for numerous discussions on the subject. Clarifying discussions of Dr J. C. Hewson of Sandia are appreciated. Partial results have been computed using the parallelized version of the code at the Arctic Region Supercomputing Center. The authors thank Dr S. M. de Bruyn Kops for providing the parallel code as well as for helpful discussions. P. S, S. M. and G. K acknowledge support provided by National Science Foundation (NSF) under Grant No. CTS-9810103 and CTS-0133925. P. S. and G. K. acknowledge partial support by the Center of Turbulence Research (CTR) at Stanford. H. P. acknowledges support by the Department of Energy (DOE) under the ASCI program.

REFERENCES

Ashurst, W. T., Kerstein, A. R., Kerr, R. M. & Gibson, C. H. 1987 Alignment of vorticity and scalar gradient with strain rate in siulated Navier-Stokes turbulence. *Phys. Fluids* **30**, 2343–2353.

Barlow, R. S. & Frank, J. H. 1998 Effects of turbulence on species mass fractions in methane/air jet flames. In *Proc. Twenty-Seventh Symp. (Intl) on Combustion*, pp. 1087–1095. Pittsburgh: The Combustion Institute.

Bilger, R. W. 1993 Conditional moment closure for turbulent reacting flow. *Phys. Fluids* **5**, 327–334.

Bray, K. N. C. & Peters, N. 1994 Laminar flamelets in turbulent flames. In *Turbulent Reacting Flows* (ed. P. A. Libby & F. A. Williams), chap. 2. Academic.

de Bruyn Kops, S. M. 1999 Numerical simulations of non-premixed turbulent combustion. PhD thesis, Mechanical Engineering Department, University of Washington, Seattle, WA.

Eswaran, V. & Pope, S. B. 1988 Direct numerical simulations of the turbulent mixing of a passive scalar. *Phys. Fluids* **31**, 506.

Favier, V. & Vervisch, L. 2001 Edge flames and partially premixed combustion in diffusion flame quenching. *Combust. Flame* **125**, 788–803.

Gibson, C. H. 1968 Fine structure of scalar fields mixed by turbulence. I. Zero-gradient points and minimal gradient surfaces. *Phys. Fluids* **11**, 2305.

Hewson, J. C. & Kerstein, A. R. 2002 Local extinction and reignition in nonpremixed turbulent $CO/H_2/N_2$ jet flames. *Combust. Sci. Tech.* **174** (5), 35–66.

Lee, Y. Y. & Pope, S. B. 1995 Nonpremixed turbulent reacting flow near extinction. *Combust. Flame* **101**, 501–528.

Lindstedt, P. R., Louloudi, S. A. & Váos, E. M. 2000 Joint scalar p.d.f. modeling of methanol piloted jet diffusion flames with comprehensive chemistry. In *Proc. Twenty-Eighth Symp. (Intl) on Combustion*, pp. 149–156. Pittsburgh: The Combustion Institute.

Mell, W. E., Nilsen, V., Kosály, G. & Riley, J. J. 1994 Investigation of closure models for nonpremixed turbulent reacting flows. *Phys. Fluids* **6**, 1331.

https://doi.org/10.1017/S0022112004001004 Published online by Cambridge University Press

Montgomery, C. J., Kosály, G. & Riley, J. J. 1993 Direct numerical simulation of turbulent reacting flow using a reduced hydrogen-oxygen mechanism. *Combust. Flame* **95**, 247.

Nilsen, V. 1998 Investigation of differentially diffusing scalars in isotropic decaying turbulence. PhD thesis, Mechanical Engineering Department, University of Washington, Seattle, WA.

Nilsen, V. & Kosály, G. 1999 Differential diffusion in turbulent reacting flows. *Combust. Flame* **117**, 493–513.

Overholt, M. R. & Pope, S. B. 1999 Direct numerical simulation of a statistically-stationary, turbulent reacting flow. *Combust. Theor. Model.* **3**, 371–408.

Peters, N. 1983 Local quenching due to flame stretch and non-premixed turbulent combustion. *Combust. Sci. Tech.* **30**, 1–17.

Peters, N. 1984 Laminar diffusion flamelet models in non-premixed turublent combustion. *Prog. Energy Combust. Sci.* **10**, 319–339.

Peters, N. 2000 *Turbulent Combustion*. Cambridge University Press.

Pitsch, H., Cha, C. M. & Fedotov, S. 2002 Flamelet modeling of non-premixed turbulent combustion with local extinction and re-ignition. *Combust. Theory Modell.* (submitted for publication).

Pitsch, H. & Fedotov, S. 2001 Investigation of scalar dissipation rate fluctuations in non-premixed turbulent combustion using a stochastic approach. *Combust. Theor. Modell.* **5**, 41–57.

Poinsot, T. & Veynante, D. 2001 *Theoretical and Numerical Combustion*. Philadelphia: R T Edwards.

Sripakagorn, P. 2002 Local extinction and reignition in turbulent nonpremixed combustion. PhD thesis, Mechanical Engineering Department, University of Washington, Seattle, WA.

Sripakagorn, P., Kosály, G. & Pitsch, H. 2000 Local extinction-reignition in turbulent non-premixed combustion. In *Annual Research Briefs*, pp. 117–128. NASA Ames, Stanford University: Center for Turbulence Research.

Sripakagorn, P., Kosály, G. & Pitsch, H. 2001 Reignition scenarios in a simulated diffusion flame. In *2nd Joint Meeting of the US Sections of the Combustion Institute*. Oakland, California: The Combustion Institute.

Turns, S. R. 1996 *An Introduction to Combustion: Concepts and Applications*. McGraw-Hill.

Xu, J. & Pope, S. B. 2000 PDF calculations of turbulent nonpremixed flames with local extinction. *Combust. Flame* **123**, 281–307.

Yeung, P. K. & Pope, S. B. 1988 An algorithm for tracking fluid particles in numerical simulations of homogeneous turbulence. *J. Comput. Phys.* **79**, 373–416.

https://doi.org/10.1017/S0022112004001004 Published online by Cambridge University Press